Energy 278 (2023) 127811

Contents lists available at ScienceDirect

Energy

journal homepage: www.elsevier.com/locate/energy

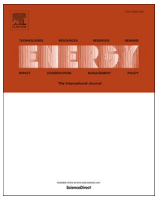

Development of selection criteria of zeotropic mixtures as working fluids for the trans-critical organic Rankine cycle

Zheng Miao [a,b], Zhanbo Wang [a], Petar Sabev Varbanov [c], Jiří Jaromír Klemeš [c], Jinliang Xu [a,b,*]

[a] Beijing Key Laboratory of Multiphase Flow and Heat Transfer, North China Electric Power University, 102206 Beijing, China
[b] Key Laboratory of Power Station Energy Transfer Conversion and System, Ministry of Education, 102206 Beijing, China
[c] Sustainable Process Integration Laboratory – SPIL, NETME Centre, Faculty of Mechanical Engineering, Brno University of Technology – VUT Brno, Technická 2896/2, 616 69, Brno, Czech Republic

ARTICLE INFO

Keywords:
Selection criteria
Trans-critical organic rankine cycle
Zeotropic mixtures
Exergy efficiency
Levelized energy cost

ABSTRACT

The *trans*-critical organic Rankine cycle (TCORC) can achieve a better thermal match in the heating process of the working fluid compared to the subcritical cycle. By using zeotropic mixtures as working fluids, the thermal match in the cooling process can be further optimized, reducing the system's irreversibility. As the selection criteria are not systematically formulated, screening zeotropic mixtures for the TCORC is challenging. In this work, the thermodynamic and thermo-economic analysis was carried out to investigate how the thermal match in the heating/cooling processes affects the system performance, which is represented by the overall exergy efficiency and the levelized energy cost. Results show that the mixture's critical temperature is a key factor influencing the system performance. Then, the mixtures having a proper condensation temperature glide can further improve the system performance. The thermo-economic analysis shows that the mixtures selected according to these criteria can also provide better thermo-economic performance, although the heat exchanger area has been enlarged during the improvement of the thermal match in heat exchangers.

1. Introduction

The increasingly severe energy shortage and environmental pollution compel people to explore more effective energy conversion technologies, among which the organic Rankine cycle (ORC) is recognized as a promising route to utilize low-to-medium grade thermal energy [1], such as biomass energy [2], geothermal energy [3], solar energy [4], and industrial waste heat [5,6], because of its simple structure and relatively high efficiency compared with other techniques, such as the thermoelectric generator [7]. The thermodynamic analysis reveals that improving the thermal match of the heat transfer processes can effectively decrease the system exergy destruction [8]. Consequently, the study on the supercritical organic Rankine cycle (SORC) [9] and the zeotropic mixture working fluid [10] has attracted wide attention. As no phase change occurs during the heating of a fluid in the supercritical state, the continuously rising fluid temperature can significantly improve the temperature match between the system and the heat source [9]. Besides, the temperature glide during the evaporation and condensation of zeotropic mixtures can also optimize the temperature match in the heating and cooling processes [11,12]. However, for most mixture working fluids, the phase-change temperature glide mainly contributes to optimizing the thermal match in the condenser rather than the evaporator because it is similar to the temperature rise of the cooling water but much smaller than the temperature drop of the heat source [13]. Using zeotropic mixtures in the TCORC can combine the advantages of these two phenomena (continuously changing temperature and condensation temperature glide), and is expected to further improve the system performance [14].

However, the selection of proper zeotropic mixtures for the TCORC is challenging as the selection criteria are not systematically formulated, which leaves a scientific gap. The screening of working fluids is an important issue in the exploration of the ORC system. Several criteria for the selection of pure working fluids have been reported in the subcritical ORC [15–17] and TCORC [18,19] and reveal that the critical temperature of the working fluid (T_{cri}) is a key factor primarily affecting the system performance. For the subcritical ORCs, Ayachi et al. [14] have reported that the suitable T_{cri} should be 33 K lower than the heat source inlet temperature (T_{hs}) while Vetter et al. [15] found that it should be 0.8 times the T_{hs}. Besides, Zhai et al. [16] gave a linear relationship between the T_{cri} and the T_{hs}. For the TCORCs, Xu et al. [18] studied the

* Corresponding author.Beijing Key Laboratory of Multiphase Flow and Heat Transfer, North China Electric Power University, 102206, Beijing, China.
E-mail addresses: miaozheng@ncepu.edu.cn (Z. Miao), xjl@ncepu.edu.cn (J. Xu).

https://doi.org/10.1016/j.energy.2023.127811
Received 3 February 2023; Received in revised form 11 April 2023; Accepted 12 May 2023
Available online 13 May 2023

ORC net power output using 12 working fluids at supercritical states. It indicated that the output power is higher when the T_{cri} is 40–65 K lower than the T_{hs}. Wang et al. [19] carried out a thermodynamic analysis of the TCORC and claimed that the lower critical temperature increases the expander outlet temperature, consequently worsening the condensation thermal match. The critical temperature in a suitable range for a given heat source condition can provide higher output power.

At present, most thermodynamic analysis of the TCORC adopts mixtures selected randomly and recommends one or more candidates according to their results [20]. The selection criteria of mixture working fluids are rarely reported [21], especially for application in TCORC. Considering the numerous types of pure substances that can be blended and the composition of the mixtures, the thermodynamic calculation bears a heavy computational load to screen the proper mixture working fluids. The reported works mainly focus on how zeotropic mixtures affected the TCORC system performance and found that the critical temperature and the condensation temperature glide were the two most important factors to optimize. Chen et al. [22] analyzed the TCORCs using R134a/R32 (0.7/0.3) and pure R134a, and found that the system thermal efficiency and heat exchanger exergy efficiencies for R134a/R32 (0.7/0.3) are both higher than pure R134a. Hærvig et al. [23] analyzed TCORC using three mixtures and suggested that the suitable mixtures should have a critical temperature 30–50 K lower than the heat source temperature. Among all the suitable mixtures, those whose condensation temperature glide close to the temperature rise of cooling water should be selected. From the works reported above, we can see that it is significant to investigate the characteristics of the TCORC using mixtures and build the selection criteria of mixture working fluid.

Besides the benefit of adopting mixtures to improve the ORC thermodynamic performance, a minor defect is that the better thermal match of the heat transfer processes requires a larger heat transfer area, consequently the higher system cost. Thus, the thermo-economic performance should also be considered when selecting zeotropic mixtures. Opposite conclusions have been drawn from the thermo-economic evaluation of the subcritical ORC with zeotropic mixtures. Some researchers found that zeotropic mixtures perform better than pure working fluid from the thermo-economic point of view [24], while others indicated a worse performance [25]. The conflicting results may be caused by that the properties of the working fluid are not matched thermally with the heat/cold source conditions. Our previous work has developed thermodynamic criteria to help select mixtures for the subcritical ORC under open and closed heat source conditions [26]. The results proved that the mixtures screened according to the criteria also exhibited relatively high thermo-economic performance [21]. Few works reported the thermo-economic analysis of the TCORC system with zeotropic mixtures. The thermo-economic analysis of the TCORC using R1234yf/R32 performed by Yang et al. [27] revealed better thermo-economic performance using mixtures than using pure R1234yf or R32.

According to the above literature, formulating selection criteria for zeotropic mixtures for the TCORC is necessary. In this work, the thermodynamic and thermo-economic analysis was carried out to study the thermal match mechanism of the heat transfer processes in the TCORC using zeotropic mixtures under the heat source without limitation on its outlet temperature (defined as the open heat source). The overall exergy efficiency is applied to measure the TCORC thermodynamic performance and develop the zeotropic mixture selection criteria, which consists of two correlations. The suitable mixtures for the TCORC system at a given heat source temperature can be screened easily and fast. The Levelized energy cost (*LEC*) is then adopted to evaluate and compare the thermo-economic performance of the TCORC.

2. The TCORC system and calculation method

Fig. 1 shows the design of the TCORC system. The equipment and numbers in the schematic is corresponding to the processes in the *T-s* diagram. The pump functions to pressurize the liquid working fluid to a supercritical pressure (5–6). Then the working fluid is heated in the evaporator (6–1) into the high-temperature/pressure supercritical fluid, which is expanded through the expander (1–2), producing output power. The low-temperature/pressure exhaust is finally cooled to the saturated or subcooled liquid in the condenser (2-3-4-5) and pumped for the next cycle.

The assumptions applied for the TCORC system are as followed:

(1) Each process of the cycle takes place at a steady state.
(2) The pressure and heat losses of heat exchangers and pipelines are neglected.
(3) The composition of the mixture is uniformly distributed in the cycle.

2.1. Thermodynamic model

The thermodynamic model of the TCORC system can be derived from the classical First and Second Laws of Thermodynamics. The detailed expressions of heat flux, exergy flow and loss, as well as the generated/consumed power of main components, are established and listed in Table 1 [28].

According to the expressions in Table 1, the exergy destruction coefficients for the processes in the TCORC system are defined as:

$$\xi_i = \frac{\dot{I}_i}{\dot{E}_{hs}}\# \tag{15}$$

The net power output, thermal efficiency, and overall exergy efficiency are calculated by:

$$\dot{W}_{net} = \dot{W}_{exp} - \dot{W}_{pump}\# \tag{16}$$

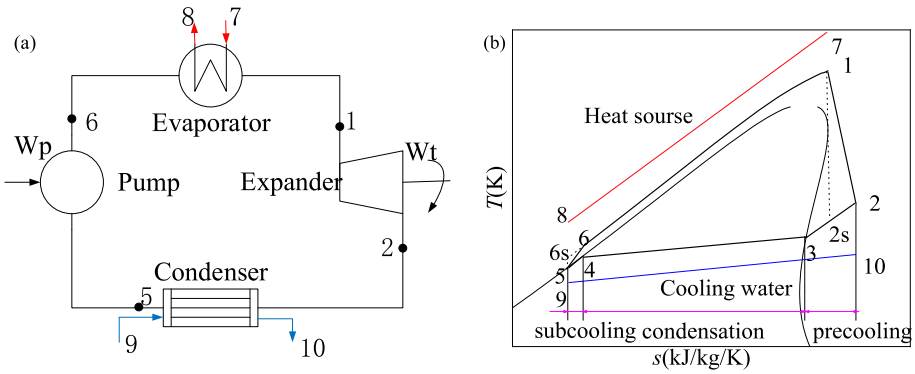

Fig. 1. Schematic and *T-s* diagrams of the TCORC system.

Table 1
Expression of the thermodynamic model.

Parameter	Calculation method	
Evaporator: Heat flux	$\dot{Q}_{hs} = \dot{m}_{wf}(h_1 - h_6) = \dot{m}_{hs}(h_7 - h_8)\#$	(1)
Heat source inlet exergy	$\dot{E}_{hs} = \dot{m}_{hs}(h_7 - h_0 - T_0(s_7 - s_0))\#$	(2)
Heat source Released exergy	$\Delta\dot{E}_{hs} = \dot{m}_{hs}(h_7 - h_8 - T_0(s_7 - s_8))\#$	(3)
Working fluid absorbed exergy	$\Delta\dot{E}_{wf\_abs} = \dot{m}_{wf}(h_1 - h_6 - T_0(s_1 - s_6))\#$	(4)
Exergy loss in the evaporator	$\dot{I}_{eva} = \Delta\dot{E}_{hs} - \Delta\dot{E}_{wf\_abs} = T_0\left(\dot{m}_{wf}(s_1 - s_6) - \dot{m}_{hs}(s_7 - s_8)\right)\#$	(5)
Heat source exergy loss	$\dot{I}_{hs} = \dot{E}_{hs} - \Delta\dot{E}_{hs} = \dot{m}_{hs}(h_8 - h_0 - T_0(s_8 - s_0))\#$	(6)
Condenser: Working fluid released exergy	$\Delta\dot{E}_{wf\_rel} = \dot{m}_{wf}(h_2 - h_5 - T_0(s_2 - s_5))\#$	(7)
Cooling water absorbed exergy	$\Delta\dot{E}_{cf} = \dot{m}_{cf}(h_{10} - h_9 - T_0(s_{10} - s_9))\#$	(8)
Exergy loss in the condenser	$\dot{I}_{con} = \Delta\dot{E}_{wf\_rel} - \Delta\dot{E}_{cf} = T_0\left(\dot{m}_{cf}(s_{10} - s_9) - \dot{m}_{wf}(s_2 - s_5)\right)\#$	(9)
Exergy loss of cold source	$\dot{I}_{cf} = \dot{m}_{cf}(h_{10} - h_0 - T_0(s_{10} - s_0))\#$	(10)
Expander: Expander shaft power	$\dot{W}_{exp} = \dot{m}_{wf}(h_1 - h_2) = \eta_{exp}\dot{m}_{wf}(h_1 - h_{2s})\#$	(11)
Exergy loss of the expander	$\dot{I}_{exp} = T_0\dot{m}_{wf}(s_2 - s_{2s})\#$	(12)
Pump: Consumed work by pump	$\dot{W}_{pump} = \dot{m}_{wf}(h_6 - h_5) = \frac{\dot{m}_{wf}(h_{6s} - h_5)}{\eta_{pump}}\#$	(13)
Exergy loss of the pump	$\dot{I}_{pump} = T_0\dot{m}_{wf}(s_6 - s_{6s})\#$	(14)

$$\eta_I = \frac{\dot{W}_{net}}{\dot{Q}_{hs}}\# \tag{17}$$

$$\eta_{II} = \frac{\dot{W}_{net}}{\dot{E}_{hs}} = 1 - \sum \xi_i\# \tag{18}$$

The overall exergy efficiency η_{II} is adopted to measure the thermodynamic performance and build the screening criteria of zeotropic mixtures for the TCORC. Then, the thermo-economic analysis is performed for these selected mixtures to evaluate their thermo-economic performance.

2.2. Thermo-economic model

The thermo-economic indicator takes into account both the thermodynamic performance and the economic cost. It can help to develop the cost-effective TCORC system. In this work, thermo-economic performance is represented by the *LEC* [29]:

$$LEC = \frac{CRF \times C_{tot} + C_{om}}{t_{op} \times \dot{W}_{net}}\# \tag{19}$$

$$C_{om} = 1.5\%C_{tot}\# \tag{20}$$

where C_{tot} is the total cost of the TCORC system, C_{om} denotes the cost of operation and maintenance, t_{op} is the running hours per year and set as 8000 h, $\dot{W}_{net}$ is the net output power calculated by Eq. (16). The *CRF* is the abbreviation of the capital recovery factor:

$$CRF = \frac{i(1+i)^{LT_{pl}}}{\left[(1+i)^{LT_{pl}} - 1\right]}\# \tag{21}$$

LT is the lifetime of the equipment and set as 20 years while i represent the interest rate and is given as 5%.

The C_{tot} in Eq. (19) needs further calculation by considering the cost of all the equipment in the TCORC system. The module costing technique [29] is applied herein to evaluate the C_{tot}:

$$C_{tot} = \left(C_{bm,pump+}C_{bm,eva} + C_{bm,exp} + C_{bm,con}\right)\frac{CEPCI_{2020}}{CEPCI_{2001}}\# \tag{22}$$

where $CEPCI_{2001} = 397$, $CEPCI_{2020} = 668.1$ [30].

The bare equipment cost [31] of each component of the TCORC is expressed as:

$$C_{bm} = C_p^0 F_{bm}\# \tag{23}$$

where C_p^0 is the equipment purchase cost only considering the operation at ambient pressure and fabricated by common materials (carbon steel). The increase in the cost due to the pressure and material is then modified by the F_{bm}:

$$\log_{10}C_p^0 = K_1 + K_2\log_{10}(Y) + K_3[\log_{10}(Y)]^2\# \tag{24}$$

$$F_{bm} = B_1 + B_2F_mF_p\# \tag{25}$$

$$\log_{10}F_p = C_1 + C_2\log_{10}(P) + C_3[\log_{10}(P)]^2\# \tag{26}$$

Y in Eq. (24) represents the area of the evaporator/condenser, the expander output power, and the power consumed by the pump. The coefficients in Eq. (24) -(26) are listed in Table 2 [32,33].

2.3. Heat exchanger model

The area of heat exchangers is calculated in this Section and provided for Eq. (24). The logarithmic mean temperature difference (LMTD) method is established:

$$A = \frac{\dot{Q}}{U\Delta T_{LM}}\# \tag{27}$$

where $\dot{Q}$, U and ΔT_{LM} are the heat flux, LMTD, and overall heat transfer coefficient, respectively.

The evaporator and condenser in the TCORC are both arranged as the counter flow shell-tube exchanger. ΔT_{LM} is given as:

$$\Delta T_{LM} = \frac{\left(T_{out}^h - T_{in}^c\right) - \left(T_{in}^h - T_{out}^c\right)}{\ln\left(\left(T_{out}^h - T_{in}^c\right)/\left(T_{in}^h - T_{out}^c\right)\right)}\# \tag{28}$$

The coefficient U is calculated by:

$$\frac{1}{U} = \frac{1}{\alpha_i}\frac{d_o}{d_i} + \frac{d_o}{2\lambda}\ln\left(\frac{d_o}{d_i}\right) + \frac{1}{\alpha_o}\# \tag{29}$$

where α is the convective heat transfer coefficient. d is the tube diameter. λ stands for the thermal conductivity of the tube wall.

Considering the phase change in the condenser, the condenser area is calculated as the sum of three regions, the liquid region, the two-phase

Table 2
TCORC equipment cost coefficient.

Equipment	K_1	K_2	K_3	B_1	B_2	C_1	C_2	C_3	F_m	F_{bm}
Evaporator	4.3247	−0.303	0.1634	1.63	1.66	0.03881	−0.1127	0.08183	1.35	/
Condenser	4.3247	−0.303	0.1634	1.63	1.66	0.03881	−0.1127	0.08183	1.35	/
Expander	3.514	0.598	0	/	/	/	/	/	/	1.5
Pump	3.514	0.598	0	1.89	1.35	−0.3935	0.3957	−0.00226	1.55	/

region, and the vapor region. Each region is then divided into smaller cells to obtain the finer temperature profiles [34]. By analyzing the temperature curves in each cell, the pinch point location can be determined. Detailed expressions of the heat transfer coefficients are listed in Appendix A.

2.4. Calculation procedure

The procedure to carry out the thermodynamic and thermo-economic calculation is shown in Fig. 2. For the specified heating/cooling source conditions, the focus is to compare the available layouts and performance of the TCORC system with different mixtures and operating parameters, seeking the optimal operating parameters for each mixture and record the performance. The convergence of the calculation is determined by the pinch point temperature difference

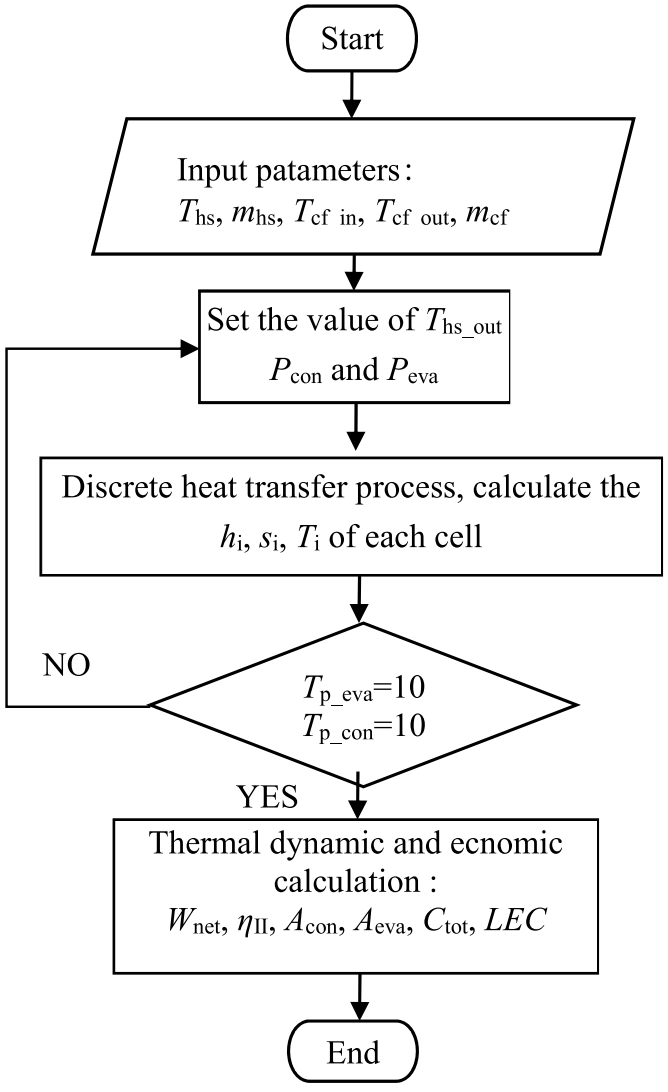

Fig. 2. The calculation procedure.

equal to 10 K, which can be realized by updating the heat source outlet temperature and condensation pressure iteratively.

The lowest fluid temperature at the expander inlet, T_1, is determined by the restriction that no liquid entrainment throughout the expander. The minimum evaporation pressure is set as 1.1 P_{cri}. Key parameters and conditions are listed in Table 3. The Matlab environment and Refprop database [35] are used for TCORC modeling.

3. Results and discussion

3.1. Heating side thermal match analysis

The mixtures used in the calculation are listed in Table 4. They are categorized into two groups, one is for data fitting, and the other is for verification. The mixtures for data fitting are all alkane mixtures because their properties have been thoroughly and accurately studied and stored in the Refprop database. However, the mixing rules for alkane with other substances, such as the Freon, or the mixing rules between Freons, are lacking. In this condition, the properties of mixtures chosen for correlation verification are estimated by a modified Helmholtz equation.

3.1.1. Effect of T_{cri} on TCORC thermodynamic performance

Previous works [15–17] have reported the finding that the T_{cri} of working fluids has a significant impact on the subcritical ORC's thermodynamic performance. In this research, we summarized the variation of η_{II} with T_{cri} at different T_{hs}, as shown in Fig. 3. Scatters in the figure represent different mixtures or mixtures with different compositions. The strong correlation between T_{cri} and T_{hs} which influences the TCORC exergy efficiency can be observed. At a certain T_{hs}, the η_{II} first increases with the increase in T_{cri}, reach the highest efficiency, then decreases with the further increase in T_{cri}. The same trends can be seen at various T_{hs}. The dashed lines in Fig. 3 stand for the mixture's optimal T_{cri} corresponding to the highest exergy efficiency. According to Eq. (2) and Eq. (18), the $\dot{E}_{hs}$ is a constant for a given heat source inlet temperature, thus the trend of η_{II} in Fig. 3 can also represent the variation of the system output power. Results in Fig. 3 agree well with the works reported by Xu et al. [18] and Wang et al. [19], which depict the variation of net output power at different heat source inlet temperatures.

The variation of η_{II} in Fig. 3 is primarily affected by the thermal match in the evaporator. Fig. 4 presents the *T-s* diagrams of TCORC with

Table 3
Parameters in the calculation.

Parameter	Unit	Value	Reference
Expander isentropic efficiency, η_{exp}	%	80	[36]
Pump efficiency , η_{pump}	%	75	[37]
Heat source		Air	
Cooling source		Water	
Pinch point temperature difference in the evaporator, $T_{p,eva}$	K	10	[38]
Pinch point temperature difference in the condenser, $T_{p,con}$	K	10	[39]
Heat source inlet temperature, T_{hs}	K	463.15–623.15	
Heat source mass flow rate, $\dot{m}_{hs}$	kg/s	10	
Cooling water inlet temperature, $T_{cf,in}$	K	293.15	[40]
Cooling water outlet temperature, $T_{cf,out}$	K	303.15	
Subcooling degree of condenser, ΔT_{sub}	K	0, 5	

Table 4
Critical temperature and pressure of the mixtures (mass fraction 0.0–1.0).

Working fluids for data fitting		
Working fluids	T_{cri} (K)	P_{cri} (kPa)
propane/isobutane	369.89–407.81	3.63–4.25
propane/butane	369.89–425.13	3.80–4.25
isobutene/isopentane	407.81–460.35	3.38–4.01
isobutene/pentane	407.81–469.7	3.37–4.01
butane/isopentane	425.13–460.35	3.38–3.80
butane/pentane	425.13–469.7	3.37–3.80
isopentane/hexane	460.35–507.82	3.03–3.38
pentane/hexane	469.7–507.82	3.03–3.37
hexane/heptane	507.82–540.13	2.74–3.03
heptane/octane	540.13–569.32	2.50–2.74
octane/nonane	569.32–594.55	2.28–2.50
Working fluids for verification		
Working fluids	T_{cri} (K)	P_{cri} (kPa)
R152a/R142b	386.41–410.26	4.06–4.52
RC318/R245fa	388.38–427.16	3.65–2.78
R142b/R141b	410.26–477.5	4.06–4.21
butane/R141b	425.13–477.5	3.80–4.21
R114/R113	418.83–487.21	3.26–3.39
R123/R113	456.83–487.21	3.39–3.66
R365mfc/hexane	460–507.82	3.03–3.27
R141b/hexane	477.5–507.82	3.03–4.21

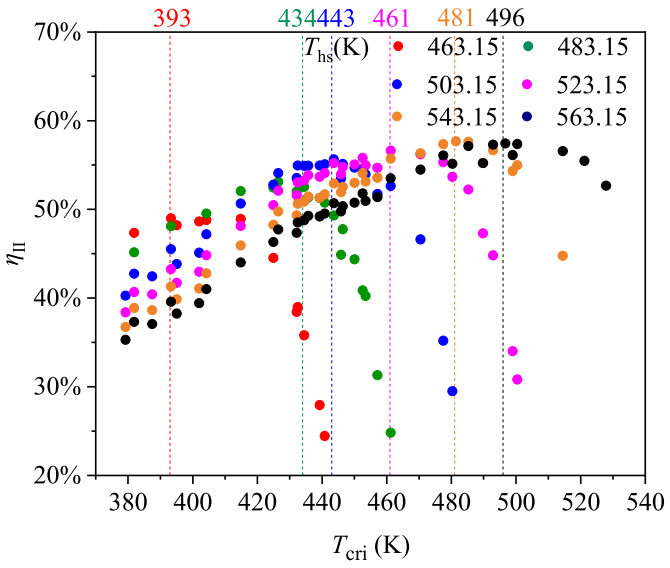

Fig. 3. Variation of the η_{II} with T_{cri} at different T_{hs}.

mixtures of different T_{cri} at the same $T_{hs,}$ and Fig. 5 exhibits the trend of exergy loss coefficients ξ_i with T_{cri} at the T_{hs} of 523.15 K. The pump and cooling water exergy loss coefficients ξ_{pump} and ξ_{cf} can be ignored as these two parts are much smaller than the others. It is seen that the pinch point is located at the inlet of the evaporator when the T_{cri} is much lower than the T_{hs} as the expander inlet pressure is set at 1.1 times the T_{cri}. Significant exergy loss is predictable according to the large gap between the temperature curves of the heat source fluid and the mixture. With the increasing T_{cri}, the expander inlet temperature becomes higher and the temperature difference becomes smaller and more uniform. Consequently, the exergy loss coefficient ξ_{eva} becomes smaller. At the same time, the exergy loss coefficients of the condenser and expander ξ_{con} and ξ_{exp} gradually increase due to the increase in the heat load of the condenser and the shaft power of the expander. However, the decrease in ξ_{eva} is more significant. As the heat source outlet temperature is relatively stable during this process, the exergy loss coefficient of the heat source ξ_{hs} remains low. As a result, an optimal T_{cri} can be found and it leads to the best thermal match, corresponding to the lowest exergy loss and the highest η_{II}. With the further increase in the T_{cri} of the

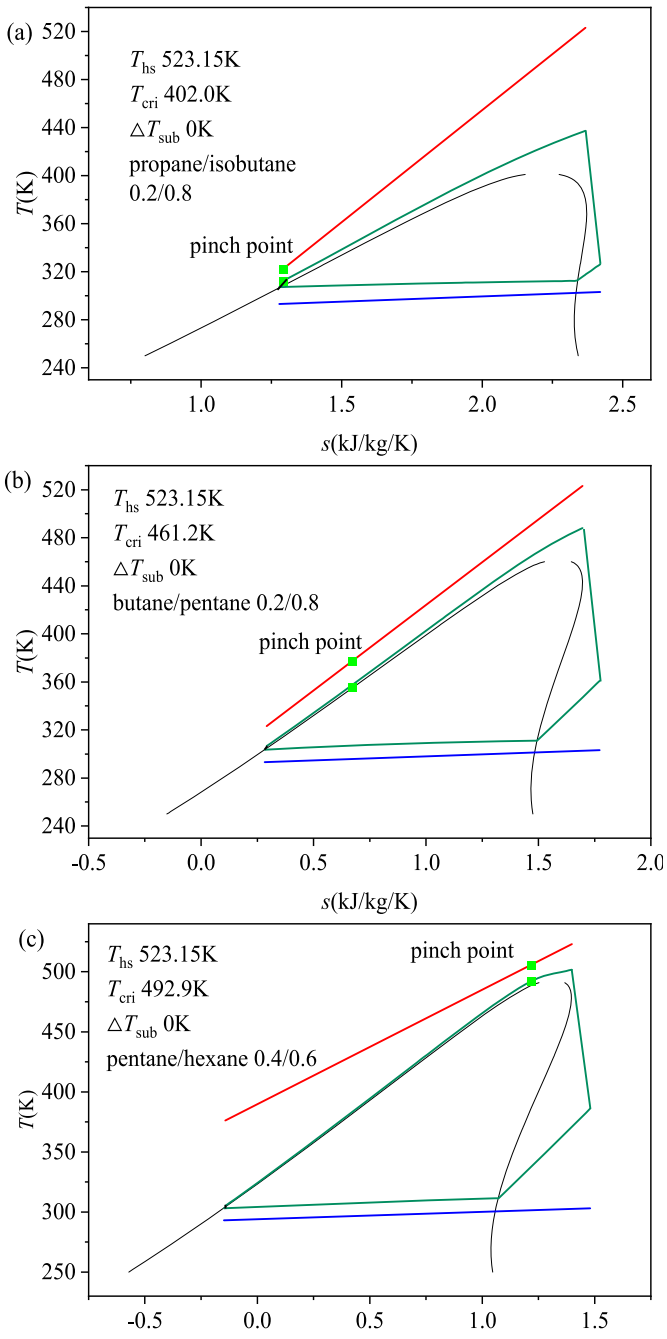

Fig. 4. *T-s* diagrams of working fluids with different T_{cri} at the same T_{hs}.

mixtures, the pinch point appears at the evaporator outlet. It is shown in Fig. 4c that the heat source outlet temperature is increased and the thermal match of the evaporator becomes worse again. The ξ_{con} and ξ_{exp} begin to decrease while ξ_{eva} and ξ_{hs} increase gradually. Results in Figs. 3 and 5 indicate that the T_{cri} of mixtures has an apparent impact on the heating side thermal match. The system exergy efficiency, η_{II}, is primarily influenced by the evaporator exergy loss coefficient ξ_{eva}. Thus, the T_{cri} can be the dominant indicator of a mixture working fluids that should be first considered during the selection.

3.1.2. *Effect of T_{cri} on TCORC thermo-economic performance*

Fig. 6 illustrates the variation of the equipment cost and the total cost with the T_{cri}. It is seen that the total cost, $C_{bm,tot}$, is mainly attributed to the cost of the evaporator and expander. The maximum $C_{bm,tot}$ is seen at a certain T_{cri}. This trend is similar to the exergy efficiency η_{II} with T_{cri} in

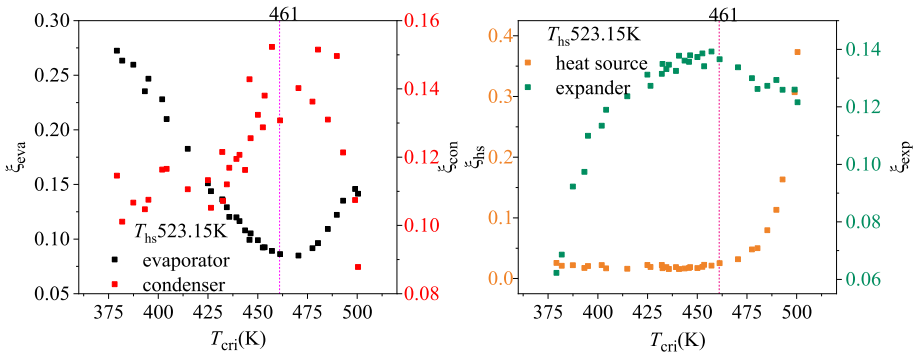

Fig. 5. Variation of the equipment exergy loss coefficient with T_{cri}.

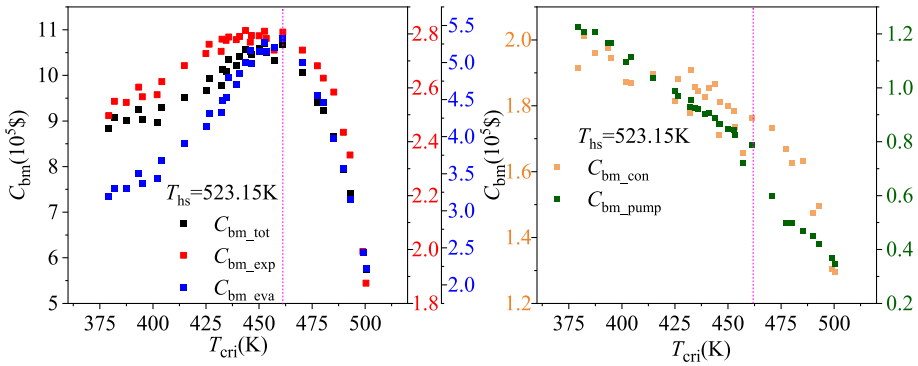

Fig. 6. Variation of the equipment costs with T_{cri}.

Fig. 3. As the η_{II} increases, the reduced temperature difference in the evaporator leads to the larger evaporator area and the expander power. Hence, the costs of the evaporator and expander are positively increased. The optimization of the heating side thermal match increases the total system cost correspondingly. The evaporator cost, C_{bm_eva}, contributes about half of the total cost and exhibits the largest variation range with the increase in the T_{cri}. It reaches a maximum at the optimal T_{cri} as the best thermal match corresponds to the minimum temperature difference. The expander cost, C_{bm_exp}, is approximately a quarter of the total cost. The trend of C_{bm_exp} varying with the T_{cri} is similar to C_{bm_eva} but within a relatively narrow range. The cost of pump and condenser C_{bm_pump} and C_{bm_con}, decrease monotonically with the increase of T_{cri}. When T_{cri} is lower than the optimal value, the heat load for the evaporator is relatively stable as the outlet temperature of the heat source varies quite gently. The increase of the expander shaft power with T_{cri} means more heat is converted into work. Consequently, the heat load of the condenser is reduced. When the T_{cri} becomes higher than the optimal value, the further increase in T_{cri} will reduce the evaporator heat load and the expander power. The continuous decline in the cost of the condenser indicates a further decrease in the condenser heat load.

As the improvement of the system exergy efficiency η_{II} has also increased the system cost, the thermo-economic performance should be further analyzed. The thermo-economic performance is represented by the *LEC* in the present work, which is a combined index taking account of both the economic performance (total cost) and thermodynamic performance (output power) of the system. The trend of *LEC* varying with T_{cri} is shown in Fig. 7 and the optimal T_{cri} is also marked by the dashed lines, like the lines in Fig. 3. The *LEC* firstly decreases with the T_{cri}, reaches a minimum, and then goes up for most T_{hs}. The *LEC* at the optimal T_{cri} is at a low level, indicating that the improvement of system thermodynamic performance plays a major role compared with the decline of the system's economic performance. Results in Fig. 7 prove that the mixtures selected according to the thermodynamic index in the present work can also provide relatively better thermo-economic performance.

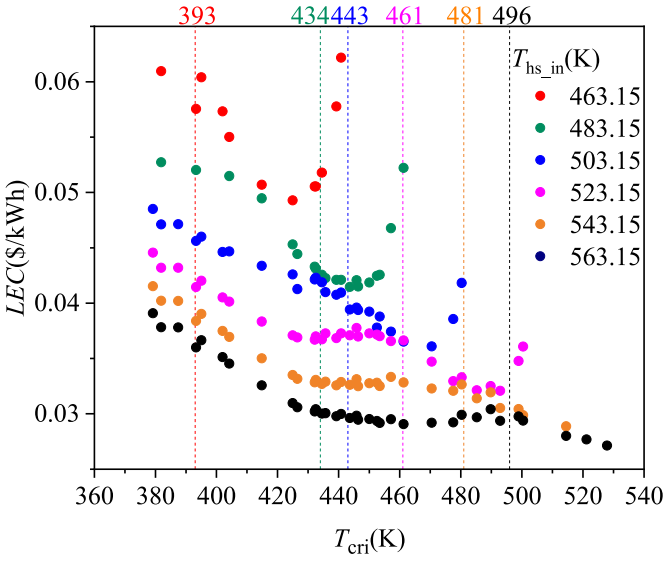

Fig. 7. Variation of the *LEC* with T_{cri} at a different T_{hs}.

3.1.3. Heating side thermal match correlation

From the former results and analysis, it is summarized that an optimal T_{cri} corresponding to the maximum η_{II} and a relatively low *LEC* can be found for each T_{hs}. Mixtures in Table 3 are adopted in the thermodynamic calculation and Table 5 shows the results. The optimal working fluids for data fitting are the selected mixtures according to the highest η_{II}. The pinch point in the heat transfer process is a critical situation affecting the thermal match of fluids in the heat exchanger [41].

Table 5
Main properties of optimal working fluids.

Optimal working fluids for data fitting				
Working fluids	Mass fraction	(T_{hs} - T_{p_eva}) (K)	T_{cri} (K)	η_{II} (%)
propane/butane	0.6/0.4	453.15	393.29	48.96
butane/pentane	0.8/0.2	473.15	434.50	54.01
butane/pentane	0.6/0.4	493.15	443.66	55.61
butane/pentane	0.2/0.8	513.15	461.25	56.63
pentane/hexane	0.7/0.3	533.15	481.40	57.61
pentane/hexane	0.3/0.7	553.15	496.69	57.36
hexane/heptane	0.7/0.3	573.15	517.82	57.35
hexane/heptane	0.3/0.7	593.15	531.20	56.49
heptane/octane	0.6/0.4	613.15	552.32	55.91
heptane/octane	0.3/0.7	633.15	562.87	54.84
Optimal working fluids for verification				
RC318/R365mfc	0.3/0.7	463.15	418.50	51.68
R114/R113	0.8/0.2	483.15	435.80	54.82
butane/R141b	0.4/0.6	503.15	447.49	56.79
R123/R113	0.4/0.6	523.15	473.55	57.70
R141b/hexane	0.8/0.2	543.15	485.18	59.91
R141b/hexane	0.2/0.8	563.15	503.10	57.46

We also considered the effect of the pinch temperature difference, T_{p_eva}. A linear correlation is achieved as Eq. (30) according to the data fitting of (T_{hs} - T_{p_eva}) vs. T_{cri} of the mixtures, represented by the black scattered points in Fig. 8.

$$T_{hs} - T_{p\_eva} = 1.10162T^*_{cri} + 6.33\ (\mathrm{K})\# \tag{30}$$

The performance of the TCORC using the 'working fluids for verification' in Table 3 is also calculated and the results are also shown in Table 5 in terms of the 'optimal working fluids for verification' and in Fig. 8 as the red scattered points. The results agree well with the fitted curve and prove the reliability of the proposed correlation. With the given T_{hs} and T_{p_eva}, the optimal T_{cri} can be determined easily with this correlation, and suitable mixtures can be found accordingly.

3.2. Cooling side thermal match analysis

By adjusting the concentration of different mixtures, various mixture working fluids with the same T_{cri} can be obtained. These mixtures have different condensation temperature glides. Thus, the condenser thermal match was further analyzed to reveal how the condensation temperature glide influences the performance of the TCORC system and determines the optimal concentrations.

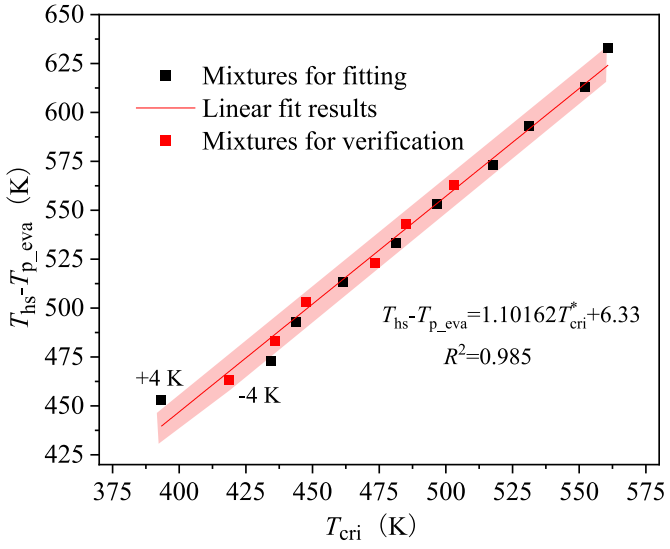

Fig. 8. Linear fitting of T_{cri} with T_{hs}-T_{p_eva}.

3.2.1. Cooling side thermal match correlation

The ideal cooling side thermal match with and without the subcooling process is shown in Fig. 9. The mixture on the cooling side is in a subcritical state. ΔT_{wf_con} is the condensation temperature glide of the mixture working fluid. ΔT_{cf} is the cooling water temperature rise, consisting of three parts, the temperature rise of the subcooling process ΔT_{cf_sub}, the condensation process ΔT_{cf_con}, and precooling process ΔT_{cf_pre}. Under the given pinch temperature difference ΔT_{p_con}, it is clear that the ideal cooling side thermal match can be achieved when the temperature curves of the working fluid and the cooling water are approximately parallel. In this condition, the optimal ΔT_{wf_con} should be:

$$\Delta T^*_{wf\_con} = \Delta T_{cf} - \Delta T_{cf\_pre} - \Delta T_{sub}\# \tag{31}$$

where the ΔT_{sub} equals none when no subcooling exists.

For the design of a TCORC system, the ΔT_{cf} and ΔT_{sub} are given parameters, thus the optimal working fluid condensation temperature glide $\Delta T^*_{wf\_con}$ can be calculated by Equation (31) when the ΔT_{cf_pre} is determined. Then, $\Delta T^*_{wf\_con}$ was used as another criterion to screen the concentration of the mixtures. The method to predict the ΔT_{wf_con} of mixture working fluid was introduced in our former work [26] as:

$$\Delta T_{wf\_con} = T_{dew} - T_{bubble}\# \tag{32}$$

$$T_{bubble} = T_{cf\_in} + \Delta T_{p\_con} + \Delta T_{sub}\# \tag{33}$$

$$T_{dew} = g(P_{con}, x = 1)\# \tag{34}$$

$$P_{con} = f(T_{bubble}, x = 0)\# \tag{35}$$

where the dew point temperature T_{dew} and the condensation pressure P_{con} can be easily obtained through the thermophysical property database with the specific T_{bubble} and mixture concentration.

As shown in Fig. 10, the working fluids can be categorized into three types, dry fluids ($ds/dT > 0$), isentropic fluids ($ds/dT \approx 0$), and wet fluids ($ds/dT < 0$) [42] according to the slope of the saturated vapor curve. For the TCORC system, the dry working fluids will lead to higher superheating degrees of vapor at the condenser inlet than the isentropic and wet working fluid, thus have a relatively higher precooling temperature rise of the cooling water ΔT_{cf_pre}.

An analysis was performed at T_{hs} of 513.15 K. The optimal T_{cri} calculated by Eq. (30) is 450.99 K. Then, eight pure working fluids with T_{cri} below 450.99 K and ten pure working fluids with T_{cri} above 450.99 K are selected, as listed in Table 6, to be blended. The concentration can be adjusted to make all the binary mixtures have the same T_{cri} at 450.99 K. In this condition, the mixtures have different ds/dT. The pre-cooling temperature rise of cooling water, ΔT_{cf_pre}, was calculated and summarized in Fig. 11. The variation of ΔT_{cf_pre} with ds/dT is in a narrow range from 0.6 to 2 K. It is noted that ΔT_{cf_pre} will become larger when the T_{hs} is higher. To apply Eq. (31) in practice, we suggest that ΔT_{cf_pre} can be set as 1.0 K when T_{hs}<513.15 K, and 2–3 K when T_{hs}>513.15 K.

The η_{II} and *LEC* of the TCORC system using the mixtures in Table 6 were also calculated and shown in Figs. 12 and 13. In this calculation, the inlet and outlet temperatures of the cooling water are kept at 293.15 K and 303.15 K. Thus, ΔT_{cf} is 10 K ΔT_{sub} is none. And ΔT_{cf_pre} is set as 1 K based on the discussion of results in Fig. 11. Consequently, the optimal condensation temperature glide $\Delta T^*_{wf\_con}$ in Eq. (31) is 9 K. The black line in Fig. 12 represents the is the $\Delta T^*_{wf\_con}$. The mixtures with higher η_{II} are near the black line. As the variation of the temperature glide is discontinuous due to the change of physical properties for different mixtures, the cooling side thermal match correlation Eq. (31) can be further modified to:

$$\Delta T_{wf\_con} = \left(\Delta T_{cf} - \Delta T_{cf\_pre} - \Delta T_{sub}\right) \pm 2\ \mathrm{K}\# \tag{36}$$

The temperature range calculated by Eq. (36) is shown in Figs. 12 and 13 as the shadow between the red lines. We can see that the

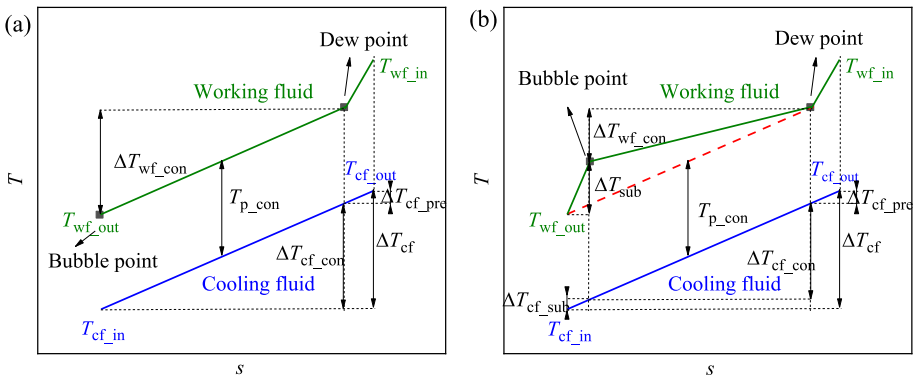

Fig. 9. Ideal cooling side thermal match.

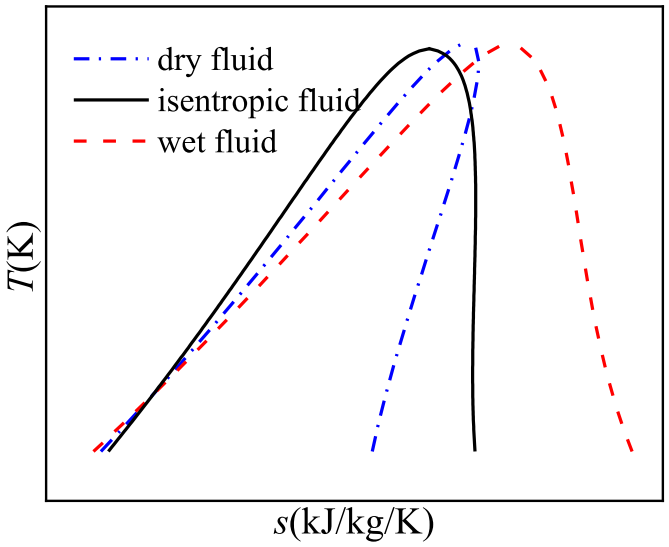

Fig. 10. *T-s* diagram of different types of working fluids.

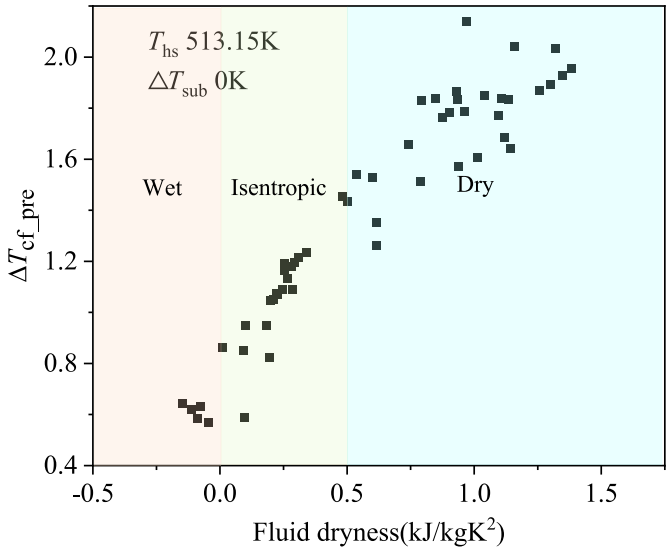

Fig. 11. Variation of the precooling temperature rise with d*s*/d*T*.

Table 6
Working fluids used for condensation correlation verification.

Working fluids' T_{cri} < optimal T_{cri}	T_{cri}(K)	Working fluids' T_{cri} > optimal T_{cri}	T_{cri}(K)
R245fa	427.16	hexane	507.82
butane	425.13	isohexane	497.7
butene	419.29	R113	487.21
R114	418.83	R141b	477.5
isobutene	418.09	R11	471.11
R142b	410.26	pentane	469.7
isobutane	407.81	isopentane	460.35
R236fa	398.07	R365mfc	460
		R123	456.83
		R21	451.48

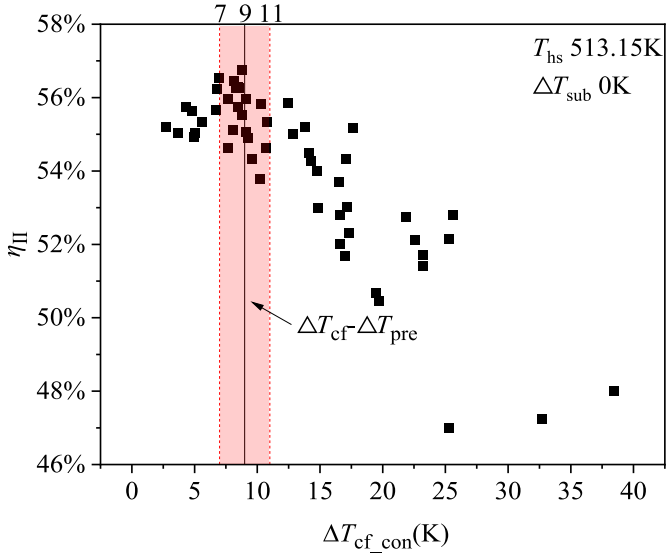

Fig. 12. Variation of the η_{II} with ΔT_{wf_con}

mixtures in this region have relatively higher exergy efficiency than other mixtures. In Fig. 13, the variation of *LEC* with ΔT_{wf_con} shows that the *LEC* at this region is lower, which means that the mixtures selected according to the cooling side thermal match correlation, Eq. (36), can provide better thermodynamic performance and thermo-economic performance at the same time.

According to the thermodynamic analysis of both the heating side and cooling side, taking the η_{II} as the optimization index, the procedure of applying these selection criteria is summarized as follows:

1) For a specified T_{hs}, the optimal critical temperature, T^*_{cri}, can be calculated by Equation (30). Choose several pure working fluids with

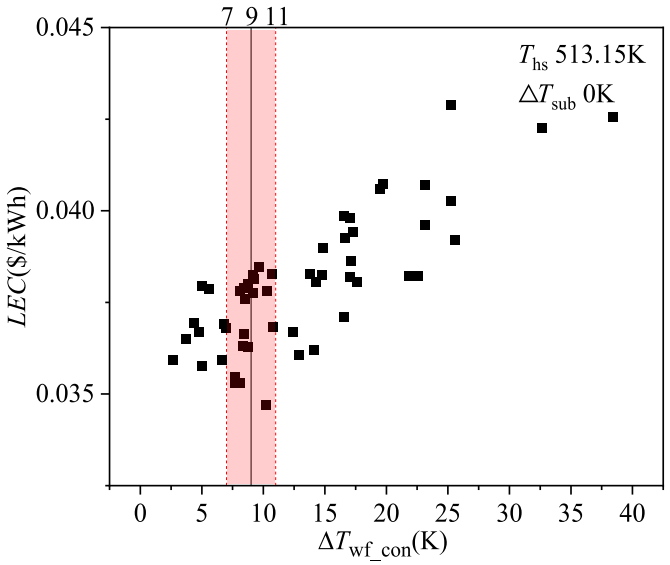

Fig. 13. Variation of the *LEC* with ΔT_{wf_con} 3.3 Procedure of the selection of mixtures for the TCORC.

T_{cri} higher and lower than the T^*_{cri} and blend them. Then various zeotropic mixtures having the same T^*_{cri} are achieved by tuning their concentration.

2) The proper ΔT_{wf_con} of the obtained mixtures is determined by Equation (36) at the given cooling water temperature rise. Then, the mixtures conforming to Equation (36) can be screened out from the zeotropic mixtures with T^*_{cri} in step 1.
3) Taking other parameters into consideration, like, toxicity, flammability, ODC, and GWP [10,43], then the suitable mixtures can be determined.

4. Conclusions

In the TCORC, the utilization of zeotropic mixture working fluids can effectively optimize the thermal matching between the system and heat/cold sources, consequently improving system performance. However, screening proper mixture working fluids for the TCORC remains challenging. In this work, the criteria for selecting zeotropic mixtures for the TCORC have been developed based on the matching mechanism between the system and heat/cold sources, studied through thermodynamic and thermo-economic analysis. It is noted that the proposed criteria are subjected to the open heat source (no limitation to the heat source outlet temperature). The mechanism of thermal matching between the TCORC and the closed heat source is quite different, and the principle of selecting mixture working fluids for the TCORC under a closed heat source needs to be further investigated. The main findings are summarized as follows:

(1) The thermal matching between the system and the heat source has a greater impact than the cooling side and should be primarily optimized. For a given T_{hs}, the critical temperature of the working fluid dominates the thermal match and influences the TCORC thermodynamic performance.
(2) Among all mixtures with the similar heating side thermal match, those with a better thermal match of the cooling side have relatively higher system exergy efficiency. Thus, the condensation temperature glide should be considered to further improve the TCORC performance.
(3) Based on the thermodynamic analysis for both evaporation and condensation processes, two expressions are proposed for the zeotropic mixture working fluid selection:

$$T_{hs} - T_{p\_eva} = 1.10162T^*_{cri} + 6.33\ (\mathrm{K})$$

$$\Delta T_{wf\_con} = \left(\Delta T_{cf} - \Delta T_{cf\_pre} - \Delta T_{sub}\right) \pm 2\mathrm{K} \begin{cases} \Delta T_{cf\_pre} = 1\mathrm{K} & T_{hs} \le 513.15\mathrm{K} \\ \Delta T_{cf\_pre} = 2\mathrm{K} & T_{hs} > 513.15\mathrm{K} \end{cases}$$

Under the given heat source/sink conditions, the optimal critical temperature and condensation temperature glide of the mixture can be determined by these two equations. Then the suitable mixtures can be easily screened.

(4) The system's total cost is mainly determined by the costs of the evaporator and expander. Optimizing the thermal match to improve the system exergy efficiency will also increase the total cost of the system. However, the working fluids selected based on the developed criteria can also provide a better thermo-economic performance, which considers both the thermodynamic performance and the cost of the system.

Credit author statement

Zheng Miao: Conceptualization, Methodology, Writing- Original draft preparation. **Zhanbo Wang**: Software, Data curation. **Petar Sabev Varbanov**: Visualization, Investigation. **Jiří Jaromír Klemeš**: Supervision.: **Jinliang Xu**: Validation, Writing- Reviewing and Editing.

Declaration of competing interest

We state that the manuscript titled as "Development of Selection Criteria of Zeotropic Mixtures as Working Fluids for the *Trans*-critical Organic Rankine Cycle" by Zheng Miao, Zhanbo Wang, Petar Sabev Varbanov, Jiří Jaromír Klemeš, and Jinliang Xu does not have any conflict of interest including any financial, personal or other relationships with other people or organizations.

Data availability

Data will be made available on request.

Acknowledgments

The authors highly appreciate the support of the National Key R&D Program of China (No. 2019YFC1907002), the National Natural Science Foundation of China (No. 51776064), and the project "Sustainable Process Integration Laboratory - SPIL", (No. CZ.02.1.01/0.0/0.0/15_003/0000456) funded by EU as "CZ Operational Programme Research, Development, and Education," Priority 1: Strengthening capacity for quality research under the collaboration agreement with Hebei University of Technology, Tianjin, China.

This paper has been dedicated to the memory of Professor Jiří Jaromír Klemeš, Head of the Sustainable process integration laboratory (SPIL), the founder and president of 26-year PRES (Process Integration for Energy Saving and Pollution Reduction) conferences. He unexpectedly passed away on January 17, 2023. His contribution has been highly appreciated, and he will be remembered in chemical engineering, energy engineering, environmental engineering, and ecological engineering.

Nomenclature

A	heat transfer area
$\dot{E}$	exergy flow rate, kW
h	specific enthalpy, kJ/kg
$\dot{I}$	exergy loss rate, kW
$\dot{m}$	mass flow rate, kg/s
P	pressure, kPa
$\dot{Q}$	heat flux, kW
s	specific entropy, kJ/(kg/K)
T	temperature, K
U	convective heat transfer coefficient, W/(m^2·K)
W	power, kW

Greek letters

η	efficiency Δ
λ	thermal conductivity
ξ	exergy loss coefficient

Subscripts

0	reference state
abs	absorption
bm	bare model
bubble	bubble point
cf	cooling water
con	condensation/condenser
cri	critical
dew	dew point
eva	evaporation/evaporator
exp	expander
hs	heat source
p	pinch point
pre	precooling or preheating
sub	subcooling
tot	total
wf	working fluid

Appendix. Heat transfer coefficients

For both the evaporator and condenser, the Kern [44] correlation is adopted to describe the single-phase shell-side convective heat transfer process:

$$Nu = 0.36Re^{0.55}Pr^{0.33}\# \tag{37}$$

The Gnielinski [45,46] correlation is applied to calculate the single-phase tube-side convective heat transfer coefficient of the supercritical mixtures in the evaporator:

$$Nu = \frac{(f/8)(Re-1000)Pr}{1+12.7\frac{f^{0.5}}{8}\left(Pr^{\frac{2}{3}}-1\right)}\# \tag{38}$$

$$f = [0.790\ln(Re)-1.64]^{-2}\# \tag{39}$$

The pure fluid condensation heat transfer coefficient is derived from the Shah [47] correlation:

$$\alpha_{TP} = \begin{cases} \alpha_l, J_V \geq 0.98(Z+0.263)-0.62 \\ \alpha_l + \alpha_{Nu}, J_V < 0.98(Z+0.263)-0.62 \end{cases}\# \tag{40}$$

where J_V is a dimensionless number given by:

$$J_V = \frac{xG}{[gd_i\rho_V(\rho_L-\rho_V)]^{0.5}}\# \tag{41}$$

Z is Shah's correlating parameter, calculated by:

$$Z = \left(\frac{1}{x}-1\right)^{0.8}Pr^{0.4}\# \tag{42}$$

$$\alpha_{\mathrm{l}}=\alpha_{\mathrm{L}}\left(1+\frac{3.8}{Z^{0.95}}\right)\left(\frac{\mu_{\mathrm{L}}}{14\mu_{\mathrm{V}}}\right)^{(0.0058+0.557\ Pr)}\# \tag{43}$$

$$\alpha_{Nu}=1.32Re_{\mathrm{L}}^{\left(-\frac{1}{3}\right)}\left[\frac{\rho_{\mathrm{L}}(\rho_{\mathrm{L}}-\rho_{\mathrm{V}})gk_{\mathrm{L}}{}^{3}}{\mu_{\mathrm{L}}{}^{2}}\right]^{\frac{1}{3}}\# \tag{44}$$

$$\alpha_{\mathrm{L}}=0.023Re_{\mathrm{L}}{}^{0.8}Pr_{\mathrm{L}}{}^{0.4}\frac{k_{\mathrm{L}}}{d_{\mathrm{i}}}\# \tag{45}$$

Then the mixture condensation heat transfer coefficient is obtained by modifying Shah's correlation through the Bell and Ghaly [48] correction correlation:

$$\frac{1}{\alpha_{\mathrm{mix}}}=\frac{1}{\alpha_{\mathrm{mono}}}+\frac{Y_{\mathrm{V}}}{\alpha_{\mathrm{V}}}\# \tag{46}$$

$$\alpha_{\mathrm{V}}=0.023\left(\frac{Gxd_{\mathrm{i}}}{\mu_{\mathrm{V}}}\right)^{0.8}Pr_{\mathrm{V}}{}^{0.4}\frac{k_{\mathrm{V}}}{d_{\mathrm{i}}}\# \tag{47}$$

$$Y_{\mathrm{V}}=xC_{\mathrm{pv}}\frac{\Delta T_{\mathrm{glide}}}{\Delta H_{\mathrm{vap}}}\# \tag{48}$$

where α_{mono} is the condensation heat transfer coefficient calculated by Shah's correlation but using the mixture's properties.

References

[1] Liu P, Shu G, Tian H. How to approach optimal practical Organic Rankine cycle (OP-ORC) by configuration modification for diesel engine waste heat recovery. Energy 2019;174:543–52.
[2] Kalina J, Świerzewski M. Identification of ORC unit operation in biomass-fired cogeneration system. Renew Energy 2019;142:400–14.
[3] Hou J, Cao M, Liu P. Development and utilization of geothermal energy in China: current practices and future strategies. Renew Energy 2018;125:401–12.
[4] Kumar A, Gupta PR, Tiwari AK, Said Z. Performance evaluation of small scale solar organic Rankine cycle using MWCNT + R141b nanorefrigerant. Energy Conversion and Management; 2022. p. 260.
[5] Gürgen S, Altın İ. Novel decision-making strategy for working fluid selection in Organic Rankine Cycle: a case study for waste heat recovery of a marine diesel engine. Energy 2022:252.
[6] Köse Ö, Koç Y, Yağlı H. Is Kalina cycle or organic Rankine cycle for industrial waste heat recovery applications? A detailed performance, economic and environment based comprehensive analysis. Process Saf Environ Protect 2022;163:421–37.
[7] Lan S, Li Q, Guo X, Wang S, Chen R. Fuel saving potential analysis of bifunctional vehicular waste heat recovery system using thermoelectric generator and organic Rankine cycle. Energy 2023:263.
[8] Chen Q, Xu J, Chen H. A new design method for Organic Rankine Cycles with constraint of inlet and outlet heat carrier fluid temperatures coupling with the heat source. Appl Energy 2012;98:562–73.
[9] Schuster A, Karellas S, Aumann R. Efficiency optimization potential in supercritical organic rankine cycles. Energy 2010;35(2):1033–9.
[10] Li Y-R, Du M-T, Wu C-M, Wu S-Y, Liu C. Potential of organic Rankine cycle using zeotropic mixtures as working fluids for waste heat recovery. Energy 2014;77:509–19.
[11] Modi A, Haglind F. A review of recent research on the use of zeotropic mixtures in power generation systems. Energy Convers Manag 2017;138:603–26.
[12] Xu W, Deng S, Zhang Y, Zhao D, Zhao L. How to give a full play to the advantages of zeotropic working fluids in organic Rankine cycle (ORC). Energy Proc 2019;158:1591–7.
[13] Dong B, Xu G, Cai Y, Li H. Analysis of zeotropic mixtures used in high-temperature Organic Rankine cycle. Energy Convers Manag 2014;84:253–60.
[14] Gao H, Liu C, He C, Xu X, Wu S, Li Y. Performance analysis and working fluid selection of a supercritical organic rankine cycle for low grade waste heat recovery. Energies 2012;5(9).
[15] Ayachi F, Ksayer EB, Zoughaib A, Neveu P. ORC optimization for medium grade heat recovery. Energy 2014;68:47–56.
[16] Vetter C, Wiemer H-J, Kuhn D. Comparison of sub- and supercritical Organic Rankine Cycles for power generation from low-temperature/low-enthalpy geothermal wells, considering specific net power output and efficiency. Appl Therm Eng 2013;51(1):871–9.
[17] Zhai HX, An QS, Shi L. Analysis of the quantitative correlation between the heat source temperature and the critical temperature of the optimal pure working fluid for subcritical organic Rankine cycles. Appl Therm Eng 2016;99:383–91.
[18] Xu H, Gao N, Zhu T. Investigation on the fluid selection and evaporation parametric optimization for sub- and supercritical organic Rankine cycle. Energy 2016;96:59–68.
[19] Wang M, Zhang J, Liu Q, Tan L. Effects of critical temperature, critical pressure and dryness of working fluids on the performance of the transcritical organic rankine cycle. Energy 2020;202:117663.
[20] Le VL, Feidt M, Kheiri A, Pelloux-Prayer S. Performance optimization of low-temperature power generation by supercritical ORCs (organic Rankine cycles) using low GWP (global warming potential) working fluids. Energy 2014;67:513–26.
[21] Miao Z, Li Z, Zhang K, Xu J, Cheng Y. Selection criteria of zeotropic mixtures for subcritical organic Rankine cycle based on thermodynamic and thermo-economic analysis. Appl Therm Eng 2020:180.
[22] Chen H, Goswami DY, Rahman MM, Stefanakos EK. A supercritical Rankine cycle using zeotropic mixture working fluids for the conversion of low-grade heat into power. Energy 2011;36(1):549–55.
[23] Hærvig J, Sørensen K, Condra TJ. Guidelines for optimal selection of working fluid for an organic Rankine cycle in relation to waste heat recovery. Energy 2016;96:592–602.
[24] Dong B, Xu G, Li T, Quan Y, Wen J. Thermodynamic and economic analysis of zeotropic mixtures as working fluids in low temperature organic Rankine cycles. Appl Therm Eng 2018;132:545–53.
[25] Oyeniyi O, Christos MJE. Thermo-Economic and Heat Transfer Optimization of Working-Fluid Mixtures in a Low-Temperature Organic Rankine Cycle System 2016;9(6):448.
[26] Miao Z, Zhang K, Wang M, Xu J. Thermodynamic selection criteria of zeotropic mixtures for subcritical organic Rankine cycle. Energy 2019;167:484–97.
[27] Yang M-H, Yeh R-H, Hung T-C. Thermo-economic analysis of the transcritical organic Rankine cycle using R1234yf/R32 mixtures as the working fluids for lower-grade waste heat recovery. Energy 2017;140:818–36.
[28] Ping X, Yang F, Zhang H, Xing C, Wang C, Zhang W, et al. Energy, economic and environmental dynamic response characteristics of organic Rankine cycle (ORC) system under different driving cycles. Energy 2022:246.
[29] Feng Y, Zhang Y, Li B, Yang J, Shi Y. Comparison between regenerative organic Rankine cycle (RORC) and basic organic Rankine cycle (BORC) based on thermoeconomic multi-objective optimization considering exergy efficiency and levelized energy cost (LEC). Energy Convers Manag 2015;96:58–71.
[30] Zhang H, Liu X, Hao R, Ba X, Liu C, Liu Y, et al. Thermodynamic and thermoeconomic analyses of the energy segmented stepped utilization of medium- and low-temperature steam based on a dual-stage organic Rankine cycle. Appl Therm Eng 2023:219.
[31] Li T, Gao R, Gao X. Energy, exergy, economic, and environment (4E) assessment of trans-critical organic Rankine cycle for combined heating and power in wastewater treatment plant. Energy Conversion and Management; 2022. p. 267.
[32] Ren X, Li J, Pei G, Li P, Gong L. Parametric and economic analysis of high-temperature cascade organic Rankine cycle with a biphenyl and diphenyl oxide mixture. Energy Conversion and Management; 2023. p. 276.
[33] Zhu Qa, Zhai Y, Wang H, Li Z. Influence of vapor generator design on thermodynamic and techno-economic performances of transcritical organic Rankine cycle. Energy Conversion and Management; 2022. p. 257.
[34] Karellas S, Schuster A, Leontaritis A-D. Influence of supercritical ORC parameters on plate heat exchanger design. Appl Therm Eng 2012;33–34:70–6.
[35] Huang Y, Chen J, Chen Y, Luo X, Liang Y, He J, et al. Performance explorations of an organic Rankine cycle featured with separating and mixing composition of zeotropic mixture. Energy 2022:257.
[36] Wang S, Liu C, Zhang S, Li Q, Huo E. Multi-objective optimization and fluid selection of organic Rankine cycle (ORC) system based on economic-environmental-sustainable analysis. Energy Conversion and Management; 2022. p. 254.

[37] Maraver D, Royo J, Lemort V, Quoilin S. Systematic optimization of subcritical and transcritical organic Rankine cycles (ORCs) constrained by technical parameters in multiple applications. Appl Energy 2014;117:11–29.
[38] Shahrooz M, Lundqvist P, Nekså P. Performance of binary zeotropic mixtures in organic Rankine cycles (ORCs). Energy Conversion and Management; 2022. p. 266.
[39] Lecompte S, Ameel B, Ziviani D, van den Broek M, De Paepe M. Exergy analysis of zeotropic mixtures as working fluids in Organic Rankine Cycles. Energy Convers Manag 2014;85:727–39.
[40] Wang M, Zhang J, Liu H. Comparison of dual-pressure organic Rankine cycle using zeotropic mixtures. Appl Therm Eng 2022:204.
[41] Kocaman E, Karakuş C, Yağlı H, Koç Y, Yumrutaş R, Koç A. Pinch point determination and Multi-Objective optimization for working parameters of an ORC by using numerical analyses optimization method. Energy Conversion and Management; 2022. p. 271.
[42] Song C, Gu M, Miao Z, Liu C, Xu J. Effect of fluid dryness and critical temperature on trans-critical organic Rankine cycle. Energy 2019;174:97–109.
[43] Bao J, Zhao L. A review of working fluid and expander selections for organic Rankine cycle. Renew Sustain Energy Rev 2013;24:325–42.
[44] Kern D. Process heat transfer. New York, USA: McGraw-Hill; 1950.
[45] Chen X, Liu C, Li Q, Wang X, Wang S. Dynamic behavior of supercritical organic Rankine cycle using zeotropic mixture working fluids. Energy 2020;191:116576.
[46] Li M-J, Xu J-L, Cao F, Guo J-Q, Tong Z-X, Zhu H-H. The investigation of thermo-economic performance and conceptual design for the miniaturized lead-cooled fast reactor composing supercritical CO2 power cycle. Energy 2019;173:174–95.
[47] Shah, Mohammed MJH, Research R. An Improved and Extended General Correlation for Heat Transfer During Condensation in Plain Tubes 2009;15(5):889–913.
[48] Bell KJ, Ghaly MA. An approximate generalized design method for multicomponent/partial condensers. AICHE Symp Ser 1973;69:72–9.